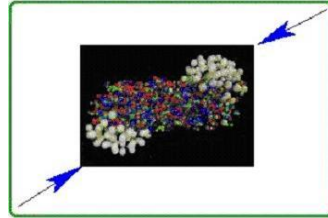EU contract number RII3-CT-2003-506395        CARE-Note-2007-019-HHH

**High Energy**

**High Intensity**

**Hadron Beams**

# Conceptual Design of Superferric Magnets for PS2

L. Bottura, R. Maccaferri, C. Maglioni, V. Parma, G. de Rijk, L. Rossi, W. Scandale, L. Serio, D. Tommasini

## Summary

*We analyze feasibility and cost of a superferric magnet design for the PS2. Specifically, we provide the conceptual design of dipole and quadrupoles, including considerations on cryogenics and powering. The magnets have warm iron yoke, and cryostated superconducting coils embedded in the magnet, which reduces AC loss at cryogenic temperature. The superconductor has large operating margin to endure beam loss and operating loads over a long period of time. Although conservative, and without any critical dependence on novel technology developments, this superconducting option appears to be attractive as a low-power alternative to the normal-conducting magnets that are the present baseline for the PS2 design. In addition it provides flexibility in the selection of flat-top duration at no additional cost.*

*This study is the conclusion of the conceptual design work started within the scope of the CARE HHH-AMT activities, following inputs from the workshops ECOMAG and LUMI-06, and finally spurred by the recent discussions on the opportunity of an R&D for the PS2 magnets.*

## Acknowledgements

## Introduction

The baseline design for the PS2 [1], [2], the upgrade of the PS injector, requires 200 dipoles totaling a magnetic length of about 600 meters, and 120 quadrupoles, for a total magnetic length of 210 m. The peak field in the dipole bore is of 1.8 T, while the peak gradient in the quadrupoles is 16 T/m. The main requirements for the magnets are summarized from [3] in Tables I and II. The operating cycle taken as a reference is the one planned for CNGS and LHC operation, reported in Fig. 1.

| PS2 main magnets | | |
|---|---|---:|
| Number of dipoles | | 200 |
| Dipole field at ejection | [T] | 1.8 |
| Dipole field at injection | [T] | 0.15 |
| Magnetic length | [m] | 2.965 |
| Bending angle | [mrad] | 31.416 |
| Number of quadrupoles | | 120 |
| Maximum gradient | [T/m] | 16 |
| Minimum gradient | [T/m] | 0.95 |
| Magnetic length | [m] | 1.75 |

Table I. Main magnet parameters for the PS2 baseline design (from [3]).

| Dipoles | $B_{nom}$ [T] | Br [Tm] | good field hor. [mm] | good field ver. [mm] | $\frac{(B-B_{nom})}{B_{nom}}$ | gap [mm] |
|---|---|---|---|---|---|---|
| Injection | 0.15 | 14.5 | ± 41.7 | ± 29.6 | $\pm\,1{\cdot}10^{-4}$ | 70 |
| Extraction | 1.80 | 170.0 | ± 41.7 | ± 11.5 | $\pm\,1{\cdot}10^{-4}$ | |

| Quadrupoles | $G_{nom}$ [T/m] | Br [Tm] | good field hor. [mm] | good field ver. [mm] | $\frac{(G-G_{nom})}{G_{nom}}$ | pole [mm] |
|---|---|---|---|---|---|---|
| Injection | 1.35 (0.95) | 14.5 | ± 50.9 | ± 36.2 | $\pm\,3{\cdot}10^{-4}$ | 75 |
| Extraction | 16.0 (11.2) | 170.0 | ± 50.9 | ± 14.0 | $\pm\,3{\cdot}10^{-4}$ | |

Table II. Aperture and field quality requirements for normal-conducting PS2 dipoles (top) and quadrupoles (bottom) (from [3]).
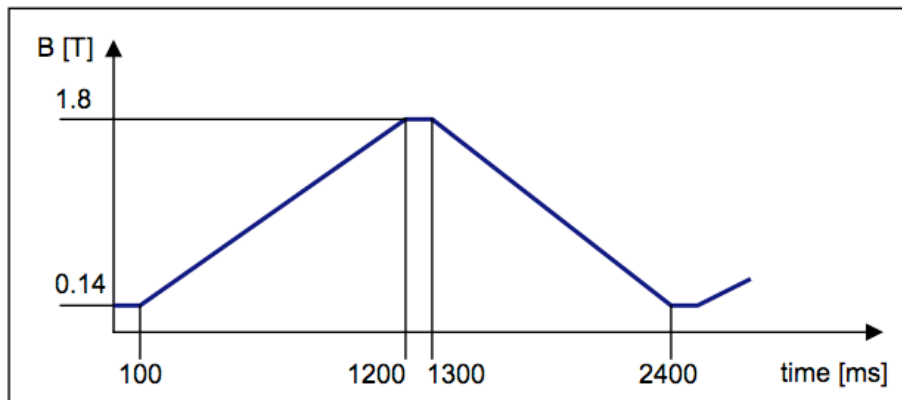


Figure 1. Reference operating cycle used for the estimation of AC loss (CNGS and LHC beams, from [3]).

The specified field range is typical of normal-conducting magnets, which is indeed the baseline for the PS2 design. With this choice, the magnet mass (dominated by the iron yoke) is considerable, in the range of 4500 tons, and the resistive power drawn from the grid is also large, around 10 MW on average. It is hence legitimate to consider the possibility of using superconducting materials to decrease the overall mass of the magnets, or the power consumption, or both. A further benefit provided by a superconducting magnet is the operational flexibility in the choice of flat-top duration longer than the nominal values shown above, at no additional operation cost.

One such study was produced by Ostojic [4], where the normal-conducting magnet design of Zickler [5] was compared to a super-ferric and to a cos-$\theta$ alternative. The main finding is that it is possible to produce a cos-$\theta$ magnet design that minimizes the amount of magnet material, reducing the dipole and quadrupole mass by nearly one order of magnitude (e.g., from 15 tons to 2 tons per dipole magnet). This solution offers a manufacturing cost advantage, estimated in [4] at 13 MCHF. The drawback of this compact design, with cold iron, is a relatively high AC loss in the superconducting coil as well as in the iron, thus requiring a large cryogenic installation, about 14 kW at 4.2 K. Following the analysis of Benedikt [6], the capital and operating cost of the cryogenic plant (26 MCHF and 4 MCHF/year respectively) offset the initial cost advantage of the superconducting magnet system, and make this alternative unattractive.

For this reason, we have re-focused the attention on an iron-dominated magnet design (dubbed here *superferric*), as initially proposed by Scandale, et al. [7]. This idea draws from the conceptual design activity that has been performed within the scope of the CARE HHH-AMT Network, aiming at cost-effective, low-field superconducting magnets for the LHC injector chain (Work Packages AMT-2 and AMT-3) [8]. Specific design targets were set at the CARE HHH-AMT workshop ECOMAG [9] and discussed at the CARE HHH-APD workshop LUMI-06 [10]. We have concluded this work, with the main aim to explore the possibility of a practical magnet design with:

- maximum efficiency in terms of power requirements and operation costs, to achieve a substantial cost gain in operation, rather than in the initial investment;
- large operating margin (electrical, mechanical, radiation) to operate reliably over a long period of time;
- minimum variations with respect to the normal-conducting baseline, to respect the boundary conditions posed by available magnet bore, access requirements and collimation.

In practice, as described in the following sections, we have taken as a starting point the normal-conducting reference magnet design and modified it to use cryostated, superconducting coils that provide the magneto-motive force. With this choice, the field quality is mainly determined by the shape of the iron pole and issues such as persistent current magnetization or conductor position accuracy are no longer of relevance. The iron yoke is warm, which is of advantage because the AC loss in the yoke no longer enters in the power balance of the cryogenic plant. Furthermore, a design with a warm iron yoke provides the same access to the magnet bore as in the normal-conducting baseline (e.g. for beam pipe and collimation systems). The coil in the dipole is removed from the magnet mid-plane, which is expected to decrease the heat load and irradiation from the particle lost from the circulating beam. Finally, the superconducting coil design selected,

based on an internally cooled cable, can be impregnated to achieve a good mechanical rigidity, the same dielectric strength as a normal-conducting winding, and a minimum helium inventory under optimal stability.

In the following sections we describe the main features of the dipole and quadrupole magnet design, providing details on the superconducting wire and cable, coil winding, cryostat design, cryogenic plant and distribution lines. We show the non-trivial result that a superferric design with warm iron can meet the field quality and operation requirements in a more compact structure than the normal-conducting baseline, requiring significantly less iron mass (approximately 50 % gain). What is most important, the AC loss during operation can be limited by design to a low value, in the range of 1 W/m of magnet. The resulting power requirements and projected operating costs are approximately half those of the normal-conducting baseline.

The harmful consequences of beam-deposited energy have been preventively treated by positioning the superconducting coils away from the mid-plane of the beam. Neither radiation resistance requirements nor beam loss estimates have been drawn so far for the baseline PS2 design. As PS2 shall provide the highest levels of reliability and robustness, we take a tentative target for that integrated radiation doses up to 10 MGy. Coil design and manufacture are compatible with this dose level. Although mandatory, a more detailed analysis of the effect of beam deposition is beyond the scope of this report.

**Magnet design**

For the design of the dipole and quadrupole magnets we have taken as a reference the study of Zickler [5].

The dipole is based on a H-type warm iron, where in our case the normal-conducting coils have been replaced by cryostated superconducting coils. Fig. 2 shows schematically this configuration. The magnetic field quality depends mainly on the pole width and on manufacturing tolerances, and is in practice not affected by cable characteristics. As for the normal-conducting option, care shall be devoted to the magnet extremities to provide a uniform field integral along the beam trajectory. The proposed magnet cross section provides the same field quality as the normal-conducting version, having the same iron pole width. With a warm iron, all material properties are identical to those of a normal-conducting magnet. In the superferric version, however, the average current density in the coil winding is about 50 A/mm$^2$, which makes it possible to place the return limbs of the yoke much closer to the magnet aperture, and thus reduce the size of the yoke. The result is that with the design of Fig. 2 it is possible to meet the dipole field quality requirements set for the PS2 with a structure weighting about 10 tons. This is considerably lighter than the 15 tons weight of a normal-conducting dipole, as shown schematically to the appropriate scale in Fig. 3. Moreover, the coils are not directly exposed to the beam, which constitutes a benefit in terms of heat load and material aging in a radiation environment.

The situation for the quadrupole is similar. The magnet cross section is shown schematically in Fig. 4, and the comparison of superferric and normal-conducting cross section is reported in Fig. 5. In the case of the quadrupoles, the iron weight is about 2.8

tons, to be compared to the 4.4 tons of the normal-conducting version, with a percentage gain similar to the case of the dipole.
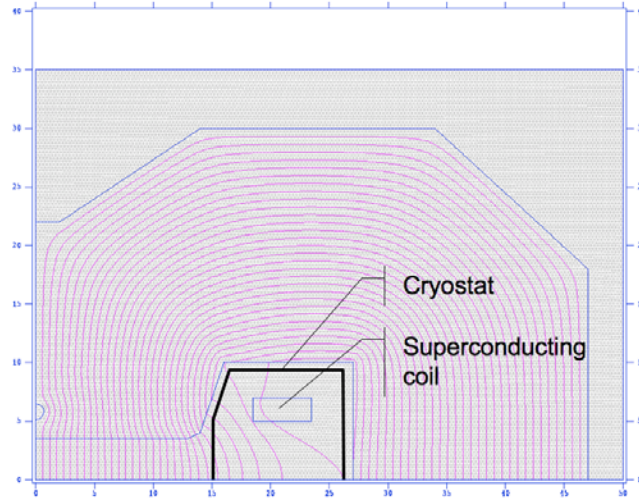


Figure 2. Transverse cross section of the superferric dipole for PS2, showing the superconducting coil winding, and the space reserved for the cryostat. The plot of the flux lines has been obtained with Poisson.
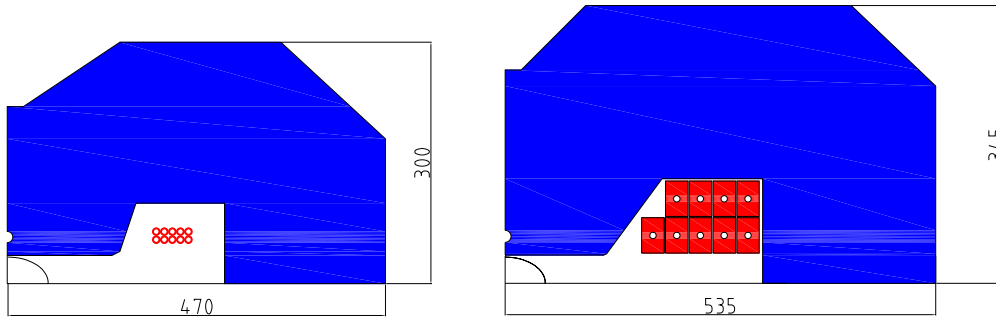


Figure 3. Comparison (to scale) of superferric (left) and normal-conducting (right) dipoles for the PS2. The normal-conducting dipole cross section has been taken from [5].
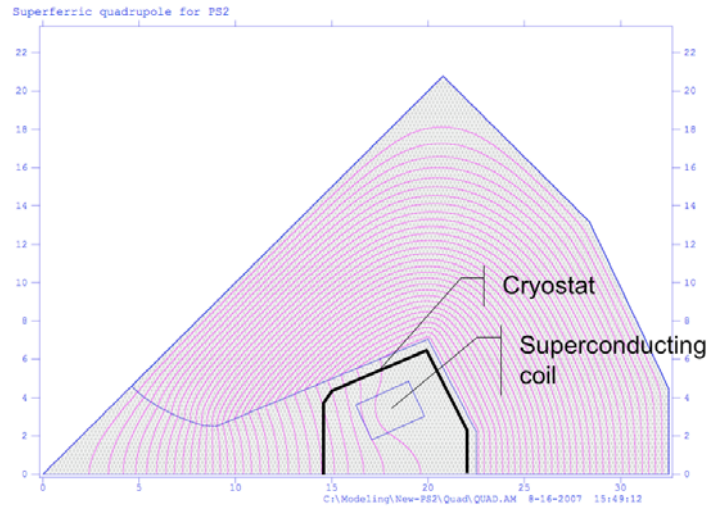


Figure 4. Transverse cross section of the superferric quadrupole for PS2, showing the superconducting coil winding, and the space reserved for the cryostat. The plot of the flux lines has been obtained with Poisson.
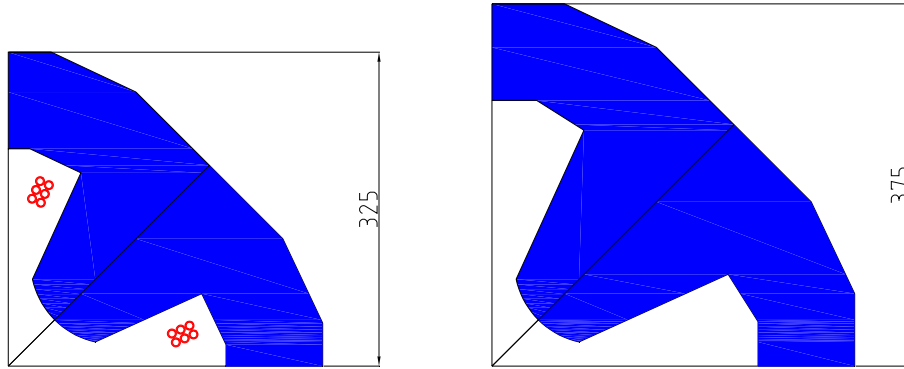
Figure 5. Comparison (to scale) of superferric (left) and normal-conducting (right) quadrupoles for the PS2. The normal-conducting quadrupole cross section has been taken from [5].

| | | Superferric | Normal-conducting |
|---|---|---|---|
| Magnet length | (m) | 3 | 3 |
| Number of turns per coil (2 coils/magnet) | (-) | 10 | 9 |
| Conductor unit length | (m) | 80 | |
| Iron weight | (tons) | 10 | 15 |
| Coil weight | (kg) | 55 | |
| Peak current @ 1.8 T | (A) | 5300 | 5775 |
| Current rise rate | (A/s) | 4830 | 5260 |
| Inductance | (mH) | 7.0 | 6 |
| Resistance | (mΩ) | 0 | 1.7 |
| RMS Current | (A) | | 3990 |
| Dissipated power | (kW) | 0 | 27 |
| Peak voltage | (V) | 34 | 41.4 |
| Horizontal force | (kN/m) | 15 | |
| Vertical force | (kN/m) | 9 | |

Table III. Main characteristics of the superferric dipole magnets. Also reported for comparison analogous parameters for the normal-conducting baseline dipole design, from [5].

In Tables III and IV we summarize the main dipole and quadrupole magnet characteristics, and report for comparison the analogous parameters (when applicable) for the normal-conducting baseline. The main differences are in mass, power consumption and operating voltage. The forces on the coil, reported in Tables III and IV for each coil pole, and per unit length, are modest (at most 15 kN/m bursting force, and 9 kN/m vertical force on the dipole coil winding).

As shown in the 2D plot of flux lines (Figs. 2 and 4), a feature of the superferric dipole and quadrupole design is that the superconducting coils experience only a relatively low magnetic field. This is a major advantage with respect to operating margin and AC loss when compared to a cable-dominated magnet such as a $\cos(n\theta)$ winding. The magnetic field was computed at nominal operating conditions, and has been reported in Table V as a map at the four corners of the winding pack. The peak field experienced by the superconductor is about a factor 2 smaller than the peak field in the magnet bore.

7

| | | Superferric | Normal-conducting |
|---|---|---|---|
| Magnet length | (m) | 1.75 | 1.75 |
| Number of turns per coil (2 coils/magnet) | (-) | 6 | 23 |
| Conductor unit length | (m) | 33 | |
| Iron weight | (tons) | 2.8 | 4.4 |
| Coil weight | (kg) | 45 | |
| Peak current @ 1.8 T | (A) | 4600 | 1200 |
| Current rise rate | (A/s) | 3830 | 1000 |
| Inductance | (mH) | 2.2 | 35 |
| Resistance | (mΩ) | 0 | 26.7 |
| RMS Current | (A) | | 830 |
| Dissipated power | (kW) | 0 | 18 |
| Peak voltage | (V) | 8 | 67 |
| Horizontal force | (kN/m) | 8 | |
| Vertical force | (kN/m) | 2 | |

Table IV. Main characteristics of the superferric quadrupole magnets. Also reported for comparison analogous parameters for the normal-conducting baseline quadrupole design, from [5].
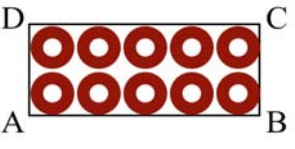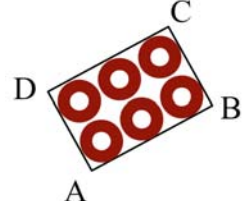
| | | dipole | quadrupole |
|---|---|---|---|
| | |  |  |
| A | (T) | 1.0 | 0.6 |
| B | (T) | 0.4 | 0.2 |
| C | (T) | 0.3 | 0.2 |
| D | (T) | 0.7 | 0.75 |

Table V. Module of the field as computed at the four corners of the superconducting coil winding (see sketch) at nominal operating conditions in the dipole and quadrupole magnets.

A further fine tuning of the magnet design would be possible, e.g. matching the operating current of dipoles and quadrupoles to reduce the complexity of the magnet interconnect and powering scheme. Although this is a viable option, we consider that an additional optimization at this stage is outside of the scope of the conceptual design study.

*Superconducting cable*

We propose to use an internally cooled conductor made with NbTi strands in one of the two alternative configurations shown in Fig. 6. The first configuration is identical as the one used for the Nuclotron cable [11], and considered the present baseline for the SIS-100 magnets of FAIR [12]. This conductor has been fabricated at JINR in Dubna (RF), and is presently commercially available at Babcock Noell Nuclear GmbH (BNN). The second configuration has been proposed as an alternative to the baseline SIS-100

conductor design, and has been object of a technology demonstration at VNIIKP (RF). The advantage of using an internally cooled conductor is that the helium is confined to the cooling pipe, which reduces greatly the helium inventory. Furthermore, apart for the terminations, the conductor can be wound using standard techniques. This is especially important, as the coil can be vacuum impregnated leading to high dielectric strength.

Table VI reports the main characteristics of the NbTi strand and of the conductor. The conductor is designed for operation at 5800 A at 4.5 K and 2 T, which is the peak field expected in the dipole aperture. Under these conditions the critical current is 15900 A, and the temperature margin to current sharing is 2.5 K, which is appropriate. We recall that the coil is placed in the low-field region of the magnet, and operates at a field which is significantly smaller than the bore field (peak field of 1 T in the dipole coil and 0.75 T in the quadrupole coil). This results in additional operating margin. In practice, the operating margin for the cable is expected to be in excess of 4 K.

The combination of the strand critical current density (minimum value of $J_c$ of 2750 A/mm$^2$ at 4.2 K and 5 T), filament diameter ($D_{eff}$ target of 2 μm) and coupling time constant (τ target of 0.5 ms) are at the high-end of what is considered today as feasible technology. In particular an effective filament diameter below 3 μm requires the use of a resistive or magnetic matrix to suppress proximity coupling and bridging of filaments, and controlled deformation to prevent filament distortion, while a coupling time constant in the range of 1 ms and below calls for resistive barriers internal to the strand to increase the transverse resistivity. A limited strand R&D is required to prove that they can be achieved simultaneously in an economic industrial process. Work in this direction is presently pursued independently by FAIR and INFN through the placement of small size purchases at European industries, and is expected to deliver relevant results within the next 12 to 24 months. In spite of this, as discussed later in the scope of the evaluation of AC loss, we have taken sufficient margin so that the magnet performance does not depend critically on an increase of either hysteresis ($D_{eff}$) or coupling loss (τ).

Table VI reports the range of acceptable values. The cable interstrand resistance, which is the last driving parameter for AC loss, is taken at 100 μΩ, i.e. in the range of values achieved for the production of the LHC cables. This is sufficient to control cable coupling loss, still maintaining good current distribution among strands.
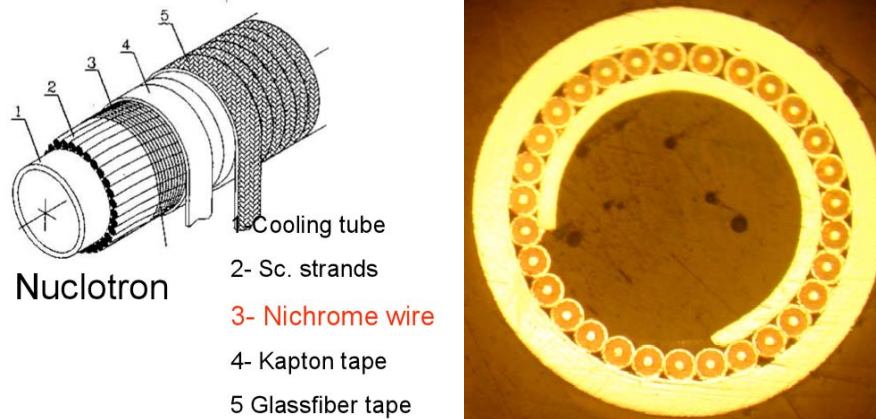


Figure 6. Cable geometries suitable for winding the coils of the superferric PS2 magnets. On the left the Nuclotron cable from JINR (RF), on the right the NCICC developed by VNIIKP (RF).

| Strand | | NbTi |
|---|---|---|
| *strand diameter* | (mm) | 0.5 |
| *Cu:NbTi* | (-) | 2.7 |
| *Jc (4.2 K, 5 T)* | (A/mm$^2$) | 2750 |
| *$D_{eff}$* | ($\mu$m) | 2…3 |
| *$\tau$* | (ms) | 0.5…1 |
| *interstrand resistance* | ($\mu\Omega$) | 100 |
| Conductor | | |
| *number of strands* | (-) | 53 |
| *conductor outer diameter* | (mm) | 9.6 |
| *operating field* | (T) | 2 |
| *operating temperature* | (K) | 4.5 |
| *operating current* | (A) | 5800 |
| *operating current density (conductor)* | (A/mm$^2$) | 80 |
| *critical current* | (A) | 15900 |
| *design current sharing temperature (5800 A, 2 T)* | (K) | 7 |
| *design temperature margin (5800 A, 2 T)* | (K) | 2.5 |
| *hydraulic diameter* | (mm) | 7.7 |

Table VI. Main strand and conductor parameters.

With the geometry above, the helium cooling channel has a diameter of 7.7 mm. To evaluate the cooling characteristics of the conductor we take a massflow of 5 g/s as a reference point, and a conductor length of 100 m, as typical of a dipole coil winding. The pressure drop necessary for the circulation is approximately 0.1 bar. Under these conditions the helium flow can remove a heat load of 0.05 W/m of conductor (i.e. 5 W total over a conductor length of 100 m) with a temperature increase of about 0.25 K. As we will discuss later, the heat removal capability is adequate for the design that we consider.

## Coil and cryostat

The coils are flat racetracks, two for the dipole and four for the quadrupole magnets, connected in series, and enclosed in a common cryostat.

Each coil is wound using the insulated, internally cooled NbTi superconducting conductor on a glass-resin coil former. After winding, the coil is wrapped with ground insulation, and impregnated under vacuum/pressure cycles, which provides high voltage withstand. This procedure is similar to that used for winding normal-conducting coils. The insulating materials are the same as used for normal-conducting magnets (fiberglass/epoxy and polyimide) and their resistance to radiation is well established. In the case of the superferric design described here, however, the coils are placed behind the iron poles, at a location where they are not exposed to direct beam radiation. This should provide a margin on the overall radiation resistance of the magnet, to be quantified. Furthermore, we have designed a comfortable space in the winding pack, with a safe distance between turns and towards ground that, together with the operation at low temperatures, should provide a remarkably long life in the accelerator environment.

Indeed, we can expect the lifetime of superconducting coils to be longer than that of normal-conducting coils.

Mechanical supporting and thermal insulating of the coils is ensured by a coil casing housed inside a vacuum vessel. The schematic cross-section in Figures 7 and 8 show conceptual solutions for the dipoles and the quadrupoles.
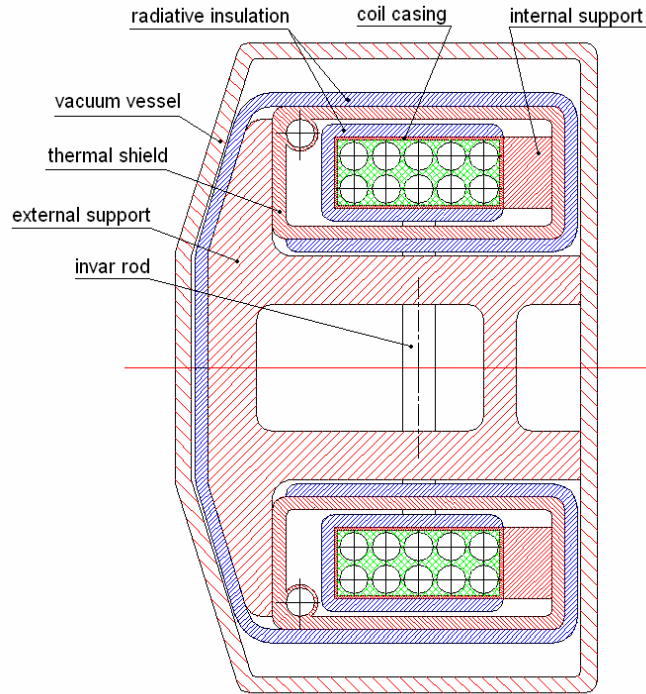


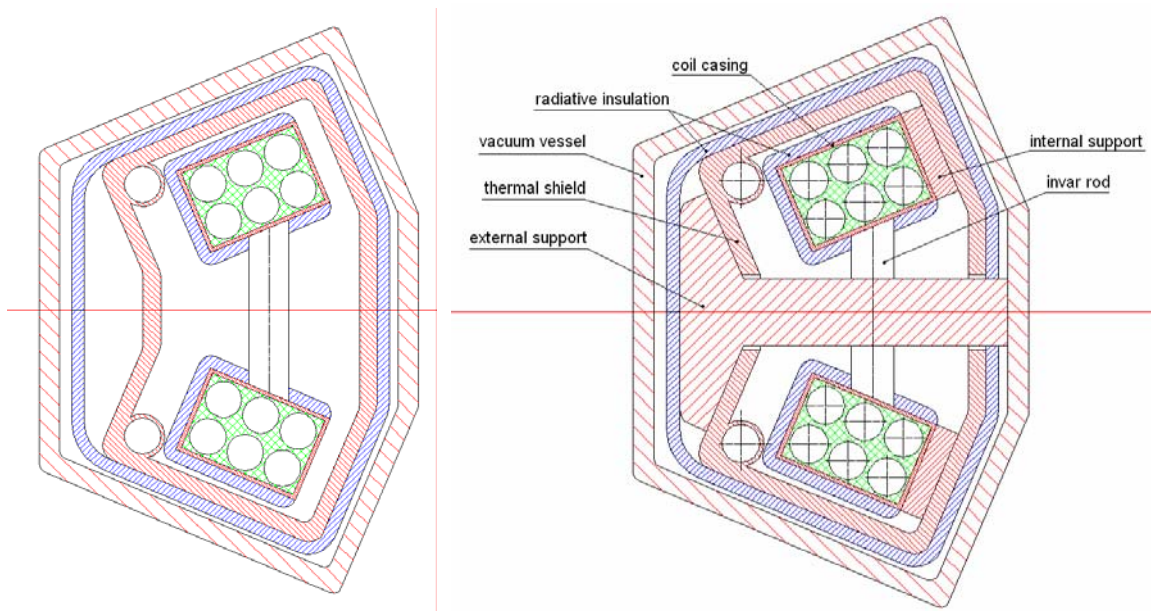Figure 7. Schematic cross section of the cryostat enclosing the dipole coils (half cross section).



Figure 8. Schematic cross section of the cryostat enclosing the quadrupole coils (quarter cross section). Two longitudinal locations are shown, showing the configuration at locations where the coil is free-standing (left) and where the coil is anchored to the external support (right)

|  | Static Heat Loads |
| --- | --- |
| @ 4.5K | 1 W/m |
| @ 75K | 2 W/m |

Table VII. Linear static heat loads, expressed per unit of magnet length, estimated for the dipole cryostat.

The supports that transfer the horizontal magnetic forces from the coil casing through the vessel wall to the iron yoke are built of low thermal conductivity material, and they are longitudinally spaced so as to limit thermal conduction heat loads while keeping the sag of the coil casing within specified limits. The top and bottom coil casings are coupled by rods at intermediate longitudinal stages to react the counteracting magnetic forces in the vertical direction. Thermal performance is enhanced by an actively cooled thermal shield at a temperature of 75 K.  Both thermal shields and coil casings are covered by a low emissivity surface protection. Space between coil casing, thermal shielding and the vessel would allow mounting 10-layer MLI blankets.

Table VII summarizes the linear static heat loads estimated for the dipole cryostats based on a simplified thermal and mechanical model where the supports are made out of a fiber-reinforced epoxy (G10CR or equivalent) designed to ensure mechanical strength and where the spacing between supports limits the sag of the coil casing to about 0.2 mm/m.


The single coils are integrated (electrical and hydraulic connections) in a *cryostated coil assembly* that forms an independent unit that can be manipulated (for assembly purposes) and powered (for test purposes) without an iron yoke. Magnet assembly and disassembly is thus simplified. This design mimics the features of a normal-conducting coil, and retains all advantages of operation and maintenance associated with the mechanical and functional split of iron yoke and coil.

## Cooling and Cryogenics

*Evaluation of thermal loads at 4.2 K*

For the evaluation of the thermal loads we have considered that the PS2 will operate continuously with the cycle represented in Fig. 1. This is a conservative assumption, as the operation will most likely alternate among different cycles, of which the one in Fig. 1 has the highest ramp-rate and duty cycle. The thermal loads considered for the design of the cryogenic plant and distribution are:

- AC loss in the cable;
- beam loss in the coil;
- static thermal loads from the shields and the supports;
- liquefaction for the current leads (3 pairs of 5 kA current leads).

AC loss in the conductor has been evaluated as the sum of three terms: filament hysteresis, strand coupling and cable coupling. Using the strand and cable parameters, and taking the field map on the coil discussed earlier, the AC loss in the conductor per cycle and per unit conductor length amount to the values in Table. VIII.

The average power dissipated by AC loss in the dipole is roughly twice as large as in the quadrupole, which is due to the lower average field in the quadrupole coil. The average

| AC loss energy/cycle | | dipole | quadrupole |
|---|---|---|---|
| *hysteresis* | (mJ/m) | 7 | 5 |
| *strand coupling* | (mJ/m) | 7 | 4 |
| *cable coupling* | (mJ/m) | 6 | 3 |
| Average AC loss power | (mW/m) | 8 | 5 |

Table VIII. Average AC loss per powering cycle and unit of conductor length, split in the contribution of filament hysteresis, strand and cable coupling.

AC loss in the magnets, obtained taking the values above and the coil winding dimensions, is 1.3 W in the dipole coil (2 poles) and 0.7 W in the quadrupole coil (4 poles). This is equivalent to a loss of 0.44 W/m of dipole magnet and 0.40 W/m of quadrupole magnet. For the evaluation of the cryogenic capacity we take a design load of 1 W/m that provides a large margin with respect to this evaluation, and covers any uncertainty in the achievable loss properties of the strand.

The beam loss in the coils is expected to be small, because the coils are intentionally placed off the machine midplane, shielded by the iron yoke. Pending a detailed evaluation of beam loss profile and magnitude, we assume that a reasonable average design target, compatible with beam quality and radiation limits, is 1 W/m of magnet.

The static heat load on the coils (from the cryostat) and on the transfer lines (from enclosure and shielding) have been estimated at a comparable value, 0.2 W/m of line. In the case of the magnets we have applied this estimate per unit length of coil winding, which results in an average value of approximately 1 W/m of magnet length.

The liquefaction requirements for the current leads have been estimated assuming an optimized operation at 0.125 g/s per kA of current (and pair of current leads). Considering steady operation at nominal conditions, and separate circuits for the dipoles, focusing quadrupoles and defocusing quadrupoles we require a total of 2 g/s of liquid helium, which corresponds approximately to 250 W of refrigeration power at 4.5 K.

The last thermal load to be considered in the balance is that on the thermal shields, operated at an intermediate temperature (the reference value chosen is 75 K). The estimate for this heat load is approximately 5 kW at 75 K for the whole installation.

*Magnet cooling*

The heat to be removed from a dipole amounts to approximately 10 W, including the margin discussed above. The cooling of the magnets can be insured by a modest flow, 5 g/s of supercritical helium in each coil, i.e. 10 g/s per dipole magnet. The hydraulic length of each flow path is approximately 80 m, and the two coils are in parallel. The temperature increase under these conditions is approximately 0.25 K, for a pressure drop of 0.07 bar.

For a quadrupole the heat load is approximately half, and we can put two coils in series in the hydraulic circuit. The hydraulic length in this case becomes approximately 66 m, i.e. comparable to that of a dipole. The temperature increase is estimated at approximately 0.1 K, for a pressure drop of 0.05 bar.

| | | | heat load at 4.2 K | heat load at 75 K |
|---|---|---|---|---|
| AC loss | 1 W/m of magnet | (W) | 810 | |
| Beam loss | 1 W/m of magnet | (W) | 810 | |
| Coil cryostat | 1 W/m of magnet | (W) | 810 | |
| Transfer lines | 0.2 W/m | (W) | 260 | |
| Current leads | 3 pairs, 2 g/s | (W) | 250 | |
| Thermal shield | 2 W/m of shield | (W) | *350*[1] | 5000 |
| **Total heat load** | | **(W)** | **3290** | |

NOTES:          [1] equivalent heat load at 4.2 K considered for the calculation of the required cryogenic power.

Table IX. Summary of cryogenic loads considered for the design of the cryoplant.

The flow enters a string of magnets (3 dipoles and a quadrupole) at 4.5 K, removes the heat under a maximum temperature increase of 1 K, and exits the magnet circuit to enter a regenerator heat exchanger, placed in a cryogenic feeder line running in parallel to the magnet circuit. The heat exchanger cools the supercritical helium back to the desired inlet condition for the next string of magnets to be cooled. This insures that the operating temperature in the magnets is everywhere below 5.5 K.

*Installed cryogenic capacity, electrical and cooling requirements*

A summary of the heat loads is reported in Table IX. The nominal capacity required at 4.2 K would be 3.3 kW. An installed capacity of 5 kW, i.e. with a relatively large margin, has been assumed for the evaluation of the cost of the installation and operation, discussed later. This is a cryogenic plant of modest size, similar to some existing and operating installations at CERN.

With the installed capacity, and taking a coefficient 250 W/W for the ratio of warm to cold power, the electrical power by the plant will be 1.25 MW. The cooling power required by cold boxes and compressors is assumed to be equal to the electrical power absorbed by the plant.

## Power Supplies requirements

The parameters in Table X summarize the requirements for the design of the power supply system. We have reported for comparison the analogous parameters that apply to the normal-conducting solution, estimated on the basis of the magnet design of [5]. The largest difference is obviously on the resistive power dissipated, which amounts to an estimate of 9.2 MW for the normal-conducting baseline, vs. a negligible amount for the superferric design.

The stored energy is about the same for both the superconducting design and the baseline normal-conducting design (22 vs. 23 MJ), which implies the same amount of storage capacitors.

With the parameters below, it is possible to power all the magnet families in the accelerator in series. The power supply can be built using modules of 2 kA, 1.5 kV each.

|  |  | Superferric | Normal-conducting |
|---|---|---|---|
| Peak voltage |  |  |  |
| *quadrupoles* | (kV) | 0.96 | 8 |
| *dipoles* | (kV) | 7 | 8.3 |
| Peak current |  |  |  |
| *quadrupoles* | (A) | 4600 | 1200 |
| *dipoles* | (A) | 5300 | 5775 |
| Stored energy |  |  |  |
| *quadrupoles* | (MJ) | 2.1 | 3 |
| *dipoles* | (MJ) | 20 | 20 |
| Peak power |  |  |  |
| *quadrupoles* | (MW) | 4.3 | 9.6 |
| *dipoles* | (MW) | 37 | 52 |
| Dissipated power |  |  |  |
| *quadrupole* | (MW) | 0 | 2.2 |
| *dipoles* | (MW) | 0 | 5.4 |

Table X. Summary of requirements for the power supply design, as computed for the superferric design considered here, and contrasted to the requirements computed for the normal-conducting baseline.

The number of modules required for the superferric design is about 2/3 that required for the normal-conducting option.

The power converters for the superferric magnets require a cooling estimated at approximately 800 kW.

## Analysis

In the analysis of the superferric design we focus on the following global indicators that driver a choice of technology:

- total installed electrical power, water cooling and ventilation capacity;
- investment cost of the magnetic system, including auxiliary systems such as cryogenics and power supplies;
- operation costs.

*Power needs*

The water cooling and ventilation requirements for a superferric PS2 are listed below. Both water cooling and ventilation are approximately half the required power for the normal-conducting PS2 baseline [6].

|  | Water cooling power |
|---|---|
| Main magnets | 0 MW |
| Power converters | 0.5 MW |
| Cryoplant | 1.3 MW |
| RF | 2 MW |
| Other systems | 3 MW |
| **Total** | **6.8 MW** |

|  | Ventilation power |
|---|---|
| Tunnel ventilation | 0.1 MW |
| Cryoplant | 0.06 MW |
| **Total** | **0.16 MW** |

The electrical power required to operate a superferric PS2 is estimated at 7.6 MW, where the single contributions are listed below. The resistive power needed to operate the magnets is taken to be negligible. RF and other systems were taken from the analysis of [6]. Power needs for water cooling were estimated scaling the data in [6], taking into account the power demand listed above. Ventilation and air conditioning powers were taken as identical to that of the normal-conducting baseline.

|  | Electrical power |
|---|---|
| Main magnets | 0 MW |
| RF | 2 MW |
| Other systems | 3 MW |
| Cryoplant | 1.3 MW |
| Water cooling station | 0.4 MW |
| Ventilation | 0.5 MW |
| Air conditioning | 0.4 MW |
| **Total** | **7.6** |

For comparison, operation of the normal-conducting PS2 would require an estimated power of 14.6 MW, i.e. nearly twice as large as for this superferric design. This result is in the expected range.

*Investment cost of the magnetic and auxiliary systems*

To make comparisons easier, and for consistency reasons, the cost has been estimated using the specific costs reported in [4] for normal-conducting and superconducting magnets.

Cost of magnet production and testing

The specific costs considered in the analysis are reported below.

|  | Specific cost |
|---|---|
| Completed warm iron yoke | 6.6 CHF/kg |
| Completed SC coil | 250 CHF/kg |
| Cryostating | 25 kCHF/magnet |
| Testing | 10 kCHF/magnet |
| Quench detection and protection | 3 kCHF/magnet |

With these assumptions, and using the data of Tables III and IV, the cost of the 200 dipole and 120 quadrupole magnets is estimated as follows:

|  | Per magnet | Total cost |
|---|---|---|
| Dipole | 106 kCHF | 21.3 MCHF |
| Quadrupole | 54.5 kCHF | 6.6 MCHF |
| Testing | 10 kCHF | 3.2 MCHF |
| Quench detection and protection | 3 kCHF | 1 MCHF |
| **Total** |  | **32.1 MCHF** |

Cost of current feeders

Pending a detailed design of this item, the cost estimate for the current feeders (feed-boxes, current leads and bus-bars) has been taken identical to that used in [4], i.e. **3 MCHF** for the complete system

Cost of cryogenics

The cost estimate for the cryogenic plant and distribution lines is reported below:

|  | Total cost |
|---|---|
| Refrigerator (5 kW @ 4.5 K) | 7 MCHF |
| Helium storage | 0.5 MCHF |
| Helium purification | 0.5 MCHF |
| Warm piping | 0.5 MCHF |
| Transfer lines | 3 MCHF |
| Controls | 1 MCHF |
| Miscellanea | 1 MCHF |
| **Total** | **13.5 MCHF** |

The main cost in this chapter is that of the 5 kW refrigerator, which is estimated at 7 MCHF. This is however only half of the total cost associated with the cryogenic installation.

Lacking an accurate estimate of the cost of civil engineering for the compressor and cold-boxes installations and buildings, we have taken the figure quoted in the study of Benedikt [6], reduced by a factor 2 because of the lower cryogenic power installed, i.e. **3.1 MCHF**.

Cost of power supplies

The cost of the power supplies was estimated in [6] at a total of 12.65 MCHF for the superconducting magnet option, based on a peak power of 30 MVA. The normal-conducting baseline, also reported in [6], had a power supply cost of 19.3 MCHF for a peak power of 62 MVA. The peak power in the superferric design described here is 41 MVA, and we estimate the cost of the power supply at **15 MCHF**.

Cooling and ventilation

Both installed water cooling and ventilation are significantly lower than in the normal-conducting baseline (see above). As a consequence we should expect a cost advantage for the superferric design that we discuss here. To simplify the estimate, we assume that the cost difference (in the range of a fraction of MCHF) has a small contribution to the overall comparison of the superferric option to the normal-conducting baseline, and we do not list a quote for this cost item.

Total investment cost

The total cost of the magnetic and auxiliary systems for a superferric design is summarized below:

|  | Total investment cost |
|---|---|
| Magnets | 32.1 MCHF |
| Current feeders | 3 MCHF |
| Cryogenics | 13.5 MCHF |
| Cryogenic buildings | 3.1 MCHF |
| Power supplies | 15 MCHF |
| **Total** | **66.7 MCHF** |

When compared to the cost estimate for a normal-conducting PS2, the superferric design is more expensive by 6 MCHF. Also this cost overhead is in the expected range.

*Operation cost*

The costs for operation are estimated taking as basis a price of 40 CHF/MWh, as quoted in [6], and assuming 6000 hours of operation per year for the accelerator systems, and 7000 hours of operation per year for the cryogenics [13]. The cost of electricity is then 1.9 MCHF/year, to which we add the cost of maintenance of the cryogenic plant, estimated at 0.3 MCHF/year (estimated as 4 % of the value of the cryoplant). The total cost is hence 2.2 MCHF/year. The table below reports these figures for reference. These values should be compared to an estimated operation cost of 3.8 MCHF/year for the normal-conducting baseline.

|  | Total operation cost |
|---|---|
| Electricity (40 CHF/MWh) | 1.9 MCHF/year |
| Cryogenics maintenance | 0.3 MCHF/year |
| **Total** | **2.2 MCHF/year** |

**Conclusions**

This study completes the activities originally launched within the scope of the CARE HHH-AMT Work packages AMT-2 and AMT-3, aiming at the conceptual design and R&D definition of a cost-effective superconducting magnet for low-field application (2 T range), revived following the impulse for the finalization of the upgrade plans for the LHC injector chain, and in particular the PS.

The superferric dipole and quadrupole magnets described in this study match all requirements of field, field ramp-rate, field quality and aperture specified for the PS2 main magnets. Because of the design chosen (warm iron, cryostated coil assembly) we expect no impact on the optics of the PS2, nor on the available space and access features that should be identical to that of the normal-conducting baseline. In particular, we have not addressed issues such as the vacuum system, or the design and location of the collimation and correction systems, because the solutions for the baseline normal-conducting PS2 should be directly applicable to the superferric option described here.

The main design effort has been directed to achieving a minimum steady and transient load on the cryogenic plant, resulting in a considerable reduction of the size and cost of the cryoplant from previous estimates. The final result is that the design described here should offer substantial savings in terms of installed power (of the order of 7 MW) and operating cost (of the order of 1.5 MCHF/year, strongly depending on the cost of electricity) when compared to the normal-conducting baseline. The price is a slight disadvantage in terms of investment cost, estimated at 6 MCHF, which could be recovered in few years of operation.

**References**

[1]     W. Bartmann, M. Benedikt, C. Carli, B. Goddard, S. Hancock, J.M. Jowett, Y. Papaphilippou, Optics Considerations for the PS2, Proceedings of PAC07, Albuquerque, NewMexico, USA, 739-741, 2007.

[2]     M. Benedikt, General Design Aspects for the PS2, in Proceedings of Third CARE–HHH–APD Workshop Towards a Roadmap for the Upgrade of the LHC and GSI Accelerator Complex 'LHC-LUMI-06', W. Scandale, T. Taylor and F. Zimmermann (eds.), CERN Yellow Report 2007-002, 117-118, 2007.

[3]     M. Benedikt, Preliminary Requirements for the Design of the PS2 Main Magnets, CERN AB- OP Note 2007-029, 13 June, 2007.

[4]     R. Ostojic, A Preliminary Analysis of the Options for the Magnet System of the PS2, CERN AT-MEL Technical Note, 1 June 2007.

[5]     T. Zickler, Design Study of Normal-Conducting Magnets for the CERN PS2, AT-MEL Technical Note, EDMS No. 855337.v2, 25 June, 2007.

[6]     M. Benedikt, PS2 – Comparison of Normal-Conducting and Super-Conducting Options, Presentation to CERN-PAF, 12 September 2007.

[7]     W. Scandale, First Configuration of a Possible Superferric option for PS2+, CERN AT-MCS Internal Note 2006-07, December 2006.

[8]     http://care-hhh.web.cern.ch/care-hhh

[9]     Proceedings of HHH-AMT  Workshop on Superconducting Pulsed Magnets for Accelerators 'ECOMAG', L. Bottura, M. Buzio and D. Tommasini (eds.), EDMS No. 819797, CARE Conf-06-036-HHH, 2006. Available at: http://ecomag-05.web.cern.ch/ecomag-05

[10]    Proceedings of Third CARE–HHH–APD Workshop Towards a Roadmap for the Upgrade of the LHC and GSI Accelerator Complex 'LHC-LUMI-06', W. Scandale, T. Taylor and F. Zimmermann (eds.), CERN Yellow Report 2007-002, 2007.

[11]    A.D. Kovalenko. Status of the Nuclotron, Proceedings of EPAC'94, London, June 1994, 161-164, 1995.

[12]    FAIR An International Accelerator Facility for Beams of Ions and Antiprotons, H. H. Gutbrod (Editor in Chief) , I. Augustin, H. Eickhoff, K.-D. Groß, W. F. Henning, D. Kraemer, G. Walter Editors, ISBN  3-9811298-0-6, EAN 978-3-9811298-0-9, September 2006.

[13]    Ph. Lebrun, Private Communication, August 2007.